https://doi.org/10.5194/essd-2021-180
Preprint. Discussion started: 21 June 2021

Open Access Earth System Science Data Discussions

Laboratory data on wave propagation through vegetation with following and opposing currents

Zhan Hu[1,2,3], Simei Lian[1,3], Huayu Wei[1,4], Yulong Li[5,*], Marcel Stive[6], Tomohiro Suzuki[6,7]

[1]School of Marine Science, Sun Yat-Sen University, and Southern Marine Science and Engineering Guangdong Laboratory (Zhuhai), Zhuhai, 519082, China
[2]Guangdong Provincial Key Laboratory of Marine Resources and Coastal Engineering, Guangzhou, 510275, China
[3]Pearl River Estuary Marine Ecosystem Research Station, Ministry of Education, Zhuhai, 519082, China
[4]Department of Ocean Science, Hong Kong University of Science and Technology, Hong Kong, China
[5]Technology Centre for Offshore and Marine, 119077, Singapore
[6]Faculty of Civil Engineering and Geosciences, Delft University of Technology, Stevinweg 1, Delft 2628 CN, the Netherlands
[7]Flanders Hydraulics Research, Berchemlei 115, Antwerp 2140, Belgium

Correspondence to: Yulong Li (li_yulong@tcoms.sg)

Abstract. Coastal vegetation has been increasingly recognized as effective buffer against wind waves. Recent studies have advanced our understanding of wave dissipation process in vegetation (WDV). In intertidal environments, waves commonly propagate into vegetation fields with underlying tidal currents, which may alter WDV, but such influence is often overlooked. The key mechanism of WDV with co-existing currents are understudied, as previous studies have drawn contradictory conclusions on the effect of following currents on WDV. Subsequent laboratory experiments have partly explained the inconsistent conclusions, but relevant data are rarely available for theoretical or modelling development. Additionally, while the vegetation drag coefficient is a key factor influencing WDV, it is rarely reported for combined wave-current flows. This paper reports a unique dataset from two flume experiments, including 668 wave-only and wave with following/opposing current tests. A variety of data including wave height, drag coefficient, in-canopy velocity and acting force on mimic vegetation stem are recorded. This dataset is expected to assist future theoretical advancement on WDV, which may ultimately lead to more accurate prediction of wave dissipation capacity of real coastal wetlands. The dataset is available from figshare (https://doi.org/10.6084/m9.figshare.13026530.v2; Hu et al., 2020) with clear instructions for reuse. The current dataset will expand with additional WDV data from ongoing as well as planned future observation in real mangrove wetlands.

1 Introduction

Coastal wetlands, such as mangroves, saltmarshes and seagrasses are increasingly recognized as effective buffers against wind waves. They can efficiently reduce incident wave height, even in storm conditions (Möller et al., 2014; van Loon-Steensma et al., 2014, 2016; Vuik et al., 2016). Therefore, ecosystem-based coastal defense systems has been proposed as a cost-effective and ecologically sound alternative to conventional coastal engineering (Temmerman et al., 2013; Arkema et al., 2017; Leonardi et al., 2018). These new coastal defense systems have been brought into practice in the Netherlands and US as a 'living shorelines' (Borsje et al., 2017; Currin, 2019), which may be adapted in many other areas around the globe.

Since the first theoretical work by Dalrymple et al., (1984), wave dissipation by vegetation (WDV) has been extensively studied through field surveys (e.g. Jadhav et al., 2013; Vuik et al., 2016; Garzon et al., 2019), laboratory experiments (e.g. Lara et al., 2016; Yao et al., 2018; He et al., 2019; Tinoco et al., 2020), theoretical and numerical models (e.g. Méndez and Losada, 2004; Losada et al., 2016; Hu et al., 2019; Suzuki et al., 2019). WDV is found to be affected by both vegetation canopy traits and hydrodynamic conditions, e.g. water depth, wave period, wave height and etc. It is generally agreed that WDV increases with vegetation density and stem stiffness, while it decreases with submergence ratio (the ratio between water depth h and canopy height h_v, Méndez & Losada, 2004; Stratigaki et al., 2011) and wave period (Cao et al., 2015).

However, the effect of underlying currents on WDV is much less understood (Garzon et al., 2019). In intertidal environments, tidal currents generally flow into the vegetation wetlands in the same direction as incident waves during flooding tide, and revise during ebb tide. Using wave as a reference, the underlying currents that flow in the same direction as waves is defined as following currents, whereas the underlying currents that flow in the oppose direction as waves is defined as opposing currents. Previous studies have drawn contradicting conclusions on whether following currents promote or suppress WDV (Li and Yan, 2007; Paul et al., 2012). A subsequent laboratory study revealed that following current can either increase or decrease WDV (Hu et al., 2014), which is determined by the ratio between imposed current velocity and amplitude of horizontal orbital velocity ($\alpha = U_c/U_w$), i.e. small velocity ratio reduces WDV, but large ratio increases WDV. The contradicting conclusions on WDV variation is largely due to a lack of comprehensive data that cover a wide range of U_c/U_w ratio. Although recent studies have improved our understanding of WDV in combined wave-current flows (Maza et al., 2015; Losada et al., 2016; Lei & Nepf, 2019), relevant datasets are still scarce for further theoretical and model development, as only a few experiments have considered the effect of underlying currents and to our knowledge none of these experimental data is available to the research community.

To understand and assess WDV, the knowledge of vegetation drag coefficient (C_D) and its variation in different flow conditions is critical. C_D was introduced to link known velocity (u, either from modelling or measurements) to the drag force exerted by vegetation stems ($F_d \sim C_D * u^2$, Morison et al., 1950), which is directly related to WDV. Thus, the determination of C_D is important to accurate WDV assessment. Its variation with characteristic hydrodynamic parameters, i.e. Reynolds number (Re) and Keulegan-Carpenter number (KC) has been extensively investigated (Nepf, 2011). C_D is commonly derived by calibration method, i.e. calibrating the C_D value to ensure the modelled WDV fits with the observation (e.g. Méndez and Losada, 2004; Li and Yan, 2007). A more recent direct measurement method has been proposed to derive C_D via analyzing synchronized F_d and u on the vegetation stems (Hu et al., 2014; Chen et al., 2018). Such method does not relay on WDV models, but is based on the original Morison equation (Morison et al., 1950). Thus, it can avoid potential errors introduced by WDV models and can be readily applied in combined current-wave conditions. However, C_D and F_d in combined current-wave flow conditions have been much less reported, especially for the cases when waves coexist with opposing currents. To our knowledge, there is no such dataset available that enables further analysis.

In this paper, we present a combined dataset composed by two flume experiments on WDV with underlying currents (Hu et al., 2020). These two experiments were conducted in 2014 and 2019, respectively (hereafter referred as E14 and E19). E14 compared WDV in waves-only and waves with following currents (Hu et al., 2014), whereas E19 further included tests of waves with opposing currents. In total, E14 conducted 314 tests and E19 conducted 354 cases with different scenarios of incident waves, imposed current, vegetation density and submergence ratio. To our knowledge, it is the first freely-assessable dataset that includes a wide range of current-wave combinations. Additionally, it includes time series data of F_D, u and C_D of each test. This dataset is expected to serve future laboratory, theoretical and numerical studies on WDV, which may eventually lead to more accurate prediction of wave dissipation efficiency of real coastal wetlands. The potential usage of this dataset and future avenues to advance our understanding are discussed.

2 Methods

2.1 Flume setup of E14

E14 was conducted in the Fluid Mechanics Laboratory at Delft University of Technology in 2014 (Hu et al., 2014). The used wave flume was 40 m long and 0.8 m wide (Figure 1a). Currents were imposed in the same direction of the wave propagation, i.e. following currents. We used stiff wooden rods that were fixed vertically on a false bottom as vegetation mimics. The length of the mimic vegetation canopy was 6 m. The height (h_v) and diameter (b_v) of the rods was 0.36 m and 0.01 m, respectively. Tested water depth (h= 0.25 m and 0.5 m) is chosen to mimic emergent and submerged conditions (Table B1). To avoid complex forcing on vegetation stems, in emergent conditions the wave crests were always lower than the top of the canopy whereas in submerged conditions the wave troughs were always higher than the the top of the canopy. In the emergent and submerged conditions, the submergence ratios (h/h_v) were 1 and 1.39, respectively. The tested stem densities were N_v=62, 139, and 556 stems/m^2, denoted as VD1, VD2 and VD3, respectively (Table B1). The mimics were placed following a regular stagger pattern (Figure B1). To measure the wave height attenuation caused by the friction of flume bed and sidewalls, control tests with no mimic stems (VD0) were also tested.

In E14, wave height variation was measured by six capacitance-type wave gauges (WG1–WG6) installed in the flume (Figure 1a). The capacitance-type wave gauges were made by Deltares and its accuracy was ±0.5% (Delft Hydraulics, 1990). Force transducers (FT1-4) were installed to measure the acting force F on 4 individual vegetation mimics along the canopy (Figure 1a and Figure A1). To minimize disturbance to the flow, all the FTs were installed underneath the false bottom. FT1 and FT3

https://doi.org/10.5194/essd-2021-180
Preprint. Discussion started: 21 June 2021

were developed by Deltares, the Netherlands, whereas FT2 and FT4 were force sensors made by UTILCELL (model 300). The output of FTs is in voltage, and it can be converted to acting force in both positive and negative direction by linear regressions. The calibration is done similar to Stewart (2004). The output value does not change with the positions of the forcing on the attached vegetation mimics, i.e. the same force gives the same value no matter where the force is acting on the mimics. Force data was sampled at 1000 Hz to capture force variation within a wave period. The accuracy of the FTs was estimated to be ±1% (Hu et al., 2014), and more details on the FTs can be found in Bouma et al., (2005). FT2 (the 2nd one in the wave direction) failed during the experiment, data from which was excluded for analysis.

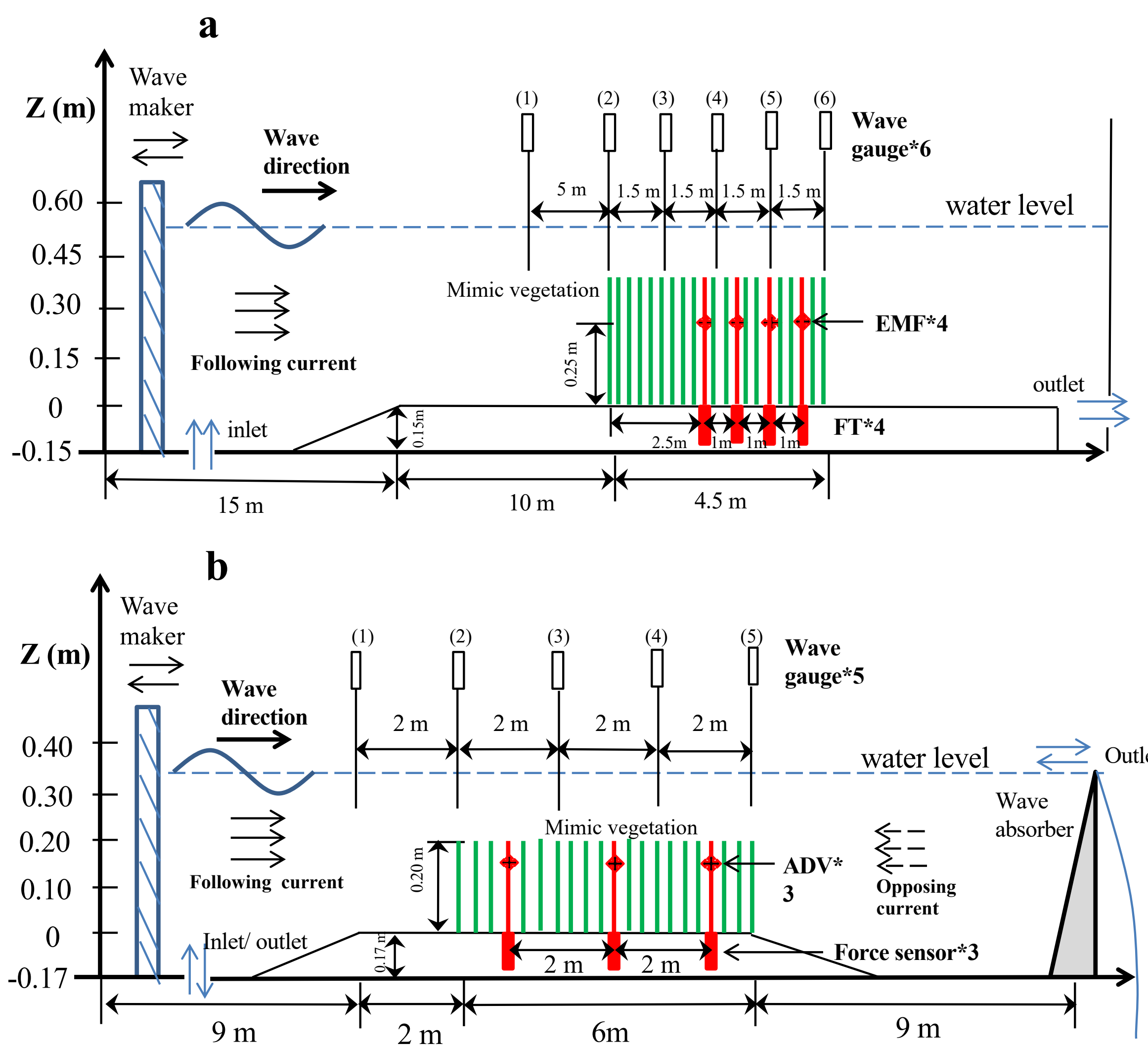

Figure 1. Diagrams of the flume experiments. (a) flume setup of E14, in which waves were imposed either with no current or with following currents. (b) flume setup of E19, in which additional tests of waves with opposing currents were included.

https://doi.org/10.5194/essd-2021-180
Preprint. Discussion started: 21 June 2021

Open Access Earth System Science Data Discussions

Velocity (u) was measured at half water depth by EMFs (electromagnetic flow manufacture meters) made by Deltares (accuracy ±1%, Delft Hydraulics, 1990). Four EMFs installed at the same cross sections as the force transducers to obtain in-phase horizontal velocity (Figure 1a), and subsequently used to derive vegetation drag coefficient (C_D). The deriving method is detailed in Appendix C. Additionally, for a few selected cases, u was measured at multiple vertical locations by moving the EMF probes to obtain velocity profiles (see Appendix B).

2.2 Flume setup of E19

E19 was conducted in the Coastal Dynamics Laboratory at Sun Yat-Sen University. As a complement to E14, E19 included cases of pure wave, wave with following currents and also wave with opposing currents. It was conducted in a 26 m long, 0.6 m wide, 0.6 m high wave flume (Figure 1b). Currents were imposed in the same and opposite direction as the wave propagation. We adapted the same vegetation canopy width and diameter as the E14. The main differences of the tested vegetation canopy were: 1) the mimic vegetation patch was 0.25 m tall; 2) low density case (VD1) of E14 was excluded, whereas VD0, VD2 and VD3 cases of E14 were retained in the E19; 3) additional tests with randomly arranged mimics (VD2R, VD3R) were included (Figure B1); 4) two water depths (h=0.2/0.33 m) were chosen to mimic emergent and submerged canopies (submergence ratio h/hv = 1 and 1.32, Table B1).

Three FT were installed to measure F acting on vegetation mimics (Figure 1b). These FTs were model M140 made by UTILCELL with an accuracy of ±1.3% (https://www.utilcell.com/en/load-cells/load-cell-m140). Their output was in mass and it can be converted to force by multiplying the acceleration of gravity. The measuring rods on FTs were made of stainless steel, so that they can be fixed tightly to the FTs (Figure A1). F was sampled at 50 Hz. Velocity (u) was measured by 3 ADVs (acoustic doppler velocimeter) at the same cross section of FTs in the canopy (Figure 1b). They were made by Nortek with an accuracy of ±0.5% (https://www.nortekgroup.com/ products/vectrino). Similar to E14, u was measured at the half of the water depth at 50 Hz. In a few selected cases, velocity profiles were obtained by moving the ADV probe vertically (see Appendix B).

In both experiments, the tested waves were regular waves. The tested wave height was 0.04-0.2 m, and wave period was 0.6-2.5 s (see Table B1). We defined the direction of wave propagation as ‘positive’ direction and the opposing direction as ‘negative’ direction. Due to Doppler Effect, the wave height could be reduced or increased when waves propagate with following and opposing currents (Demirbilek et al., 1996). For tests with same wave conditions but different co-existing currents, we adjusted the wave input to ensure the wave height arrived at the vegetation front is similar in each test with different co-existing current velocity (Hu et al., 2014). This treatment is to 1) avoid possible influenced caused by different incident wave height, and 2) reflect field conditions with similar incident wave height but with various underlying tidal currents (Garzon et al., 2019).

https://doi.org/10.5194/essd-2021-180
Preprint. Discussion started: 21 June 2021

2.3 Data analysis

In both experiments, we measured spatial wave height change, time series of acting force on vegetation mimic (F) and velocity at the middle water depth (u) as an approximation of the depth-averaged velocity (Hu et al., 2014). Following Morison equation (Morison, 1950), F on a vegetation mimic can be specified as:

$$F = F_D + F_M = \frac{1}{2}\rho C_D h_v b_v u|u| + \frac{\pi}{4}\rho C_M h_v b_v^2 \frac{\partial u}{\partial t} \quad (1)$$

F_D and F_M are drag force and inertia force, respectively. C_M is the inertia coefficient, which value is equal to 2 for cylinders (Dean and Dalrymple, 1991). ρ is the density of water. u is the depth-averaged horizontal flow velocity, and it is assumed to be equal to the flow velocity at half water depth (Hu et al., 2014). Using known u and C_D, F can be reproduced by Eq. (1). u can be decomposed as:

$$u(t) = U_{mean} + U_w \sin(\omega t) + U' \quad (2)$$

where ω is the wave angular frequency, U' is turbulent velocity fluctuations, which is neglected in the analysis for simplicity. U_{mean} is the averaged velocity over a wave period (T), defined as (e.g. Pujol et al., 2013):

$$U_{mean} = \frac{1}{T}\int_0^T U(t)dt \quad (3)$$

Please note that U_{mean} is not equal to U_c, which is the imposed current velocity without the influence of waves. U_w is the amplitude of the horizontal wave orbital velocity and can be defined as:

$$U_w = \frac{1}{2}(u_{max} - u_{min}) \quad (4)$$

where u_{max} and u_{min} are the peak flow velocities in the positive and negative directions in a wave period (T). To accommodate empirical KC-C_D relations, KC number is defined as following (Chen et al., 2018):

$$KC = \frac{Max(|u_{max}|, |u_{min}|) * T}{b_v} \quad (5)$$

Wave height (H) along the mimic vegetation canopy can be descried as:

$$K_v = \frac{H}{H_0} = \frac{1}{1+\beta x} \quad (6)$$

H_0 is the wave height at the canopy front. x is the distance into the canopy and β is a damping coefficient, which can be obtained by fitting Eq. (6). To reveal the effect of co-existing currents, the relative wave height decay in current-wave and wave-only case r_w is defined as:

$$r_w = \frac{\Delta H_{cw}}{\Delta H_{pw}} \quad (7)$$

where the ΔH_{pw} and ΔH_{cw} is the wave height reduction in pure wave and current-wave cases.

3 Data

3.1 wave dissipation in vegetation canopy with following and opposing currents

For pure wave cases, WDV in both experiments has similar variation. Emergent and denser canopies result in greater WDV than submerged and sparser canopies (Figure 2a and 1b). Additionally, such variation can also be found in the randomly

https://doi.org/10.5194/essd-2021-180
Preprint. Discussion started: 21 June 2021

Open Access Earth System Science Data Discussions

distributed vegetation canopy. No apparent difference can be found between regular and random canopies (Figure 2c). In waves plus following current cases, the two experiments also show similar results in WDV (Figure 2d and 2e). When the following current is small (0.05 m/s for E14 and 0.03 m/s for E19), the accompany currents slightly reduce WDV comparing to the pure wave cases. However, as following current velocity increases (0.15 m/s for E14 and 0.12 m/s for E19), WDV is increased compared to the pure wave cases. WDV may be further enhanced by stronger following current (0.20 m/s for E14 and 0.15 m/s for E19). As a contrast, opposing currents immediately increase WDV even when the velocity magnitude is small (Figure 2f). As the opposing current velocity increases, the WDV is promoted to a higher level comparing to the cases with following current.

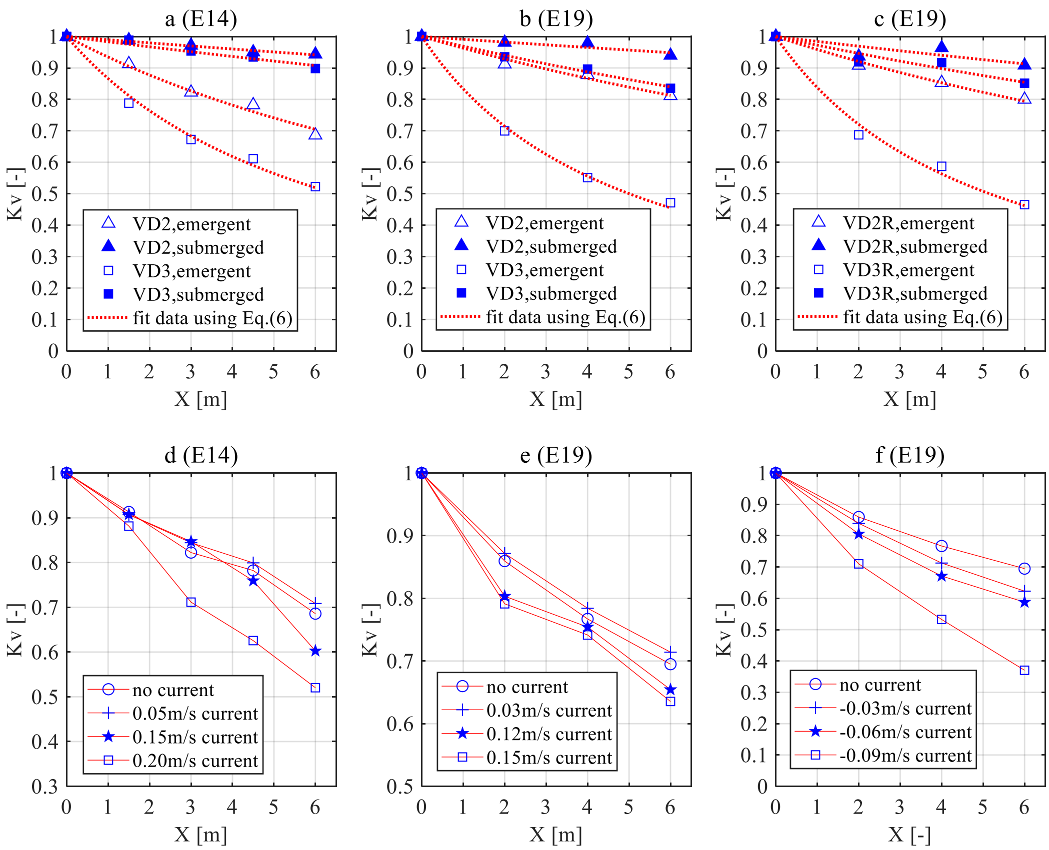

Figure 2. Relative wave height (K_v) variation through vegetation canopies (X=0-6 m). (a) K_v reduction by regular vegetation mimics in pure wave conditions in E14. The tested wave height is 4 cm and wave period is 1.0 s (i.e. wave0410); (b) K_v reduction by regular vegetation mimics in pure wave conditions in E19. The tested wave condition is wave0308; (c) K_v reduction by randomly disputed vegetation mimics in pure wave conditions in E19. The tested wave condition is wave0308; (d) K_v reduction with following currents in E14. The tested wave condition is wave0410; (e) K_v reduction with following currents in E19. The tested wave condition is wave0510; (f) K_v reduction with opposing currents in E19. The tested wave condition is wave0510. Note the different scale of the Y-axis in d-f.

The results of the two experiments present a synthesis of WDV variation with underlying currents (Figure 3). In cases with following currents, the relative wave height decay (r_w, ratio of wave height decay between current-wave and wave-only case)

https://doi.org/10.5194/essd-2021-180
Preprint. Discussion started: 21 June 2021

has similar variation in E14 and E19. When α is in the range of [0 1], r_w is generally lower than 1, i.e. WDV is suppressed compared to the pure wave cases. As a contrast, when α is larger than 1, r_w is generally larger than 1, i.e. WDV is enhanced instead. As a contrast, negative α leads to higher r_w compared to positive α with the same magnitude. Thus, opposing currents can more easily increase WDV compared to following currents. Notably, r_w value can reach 4-5 with both following and opposing currents, highlighting the impact of underlying currents on WDV.

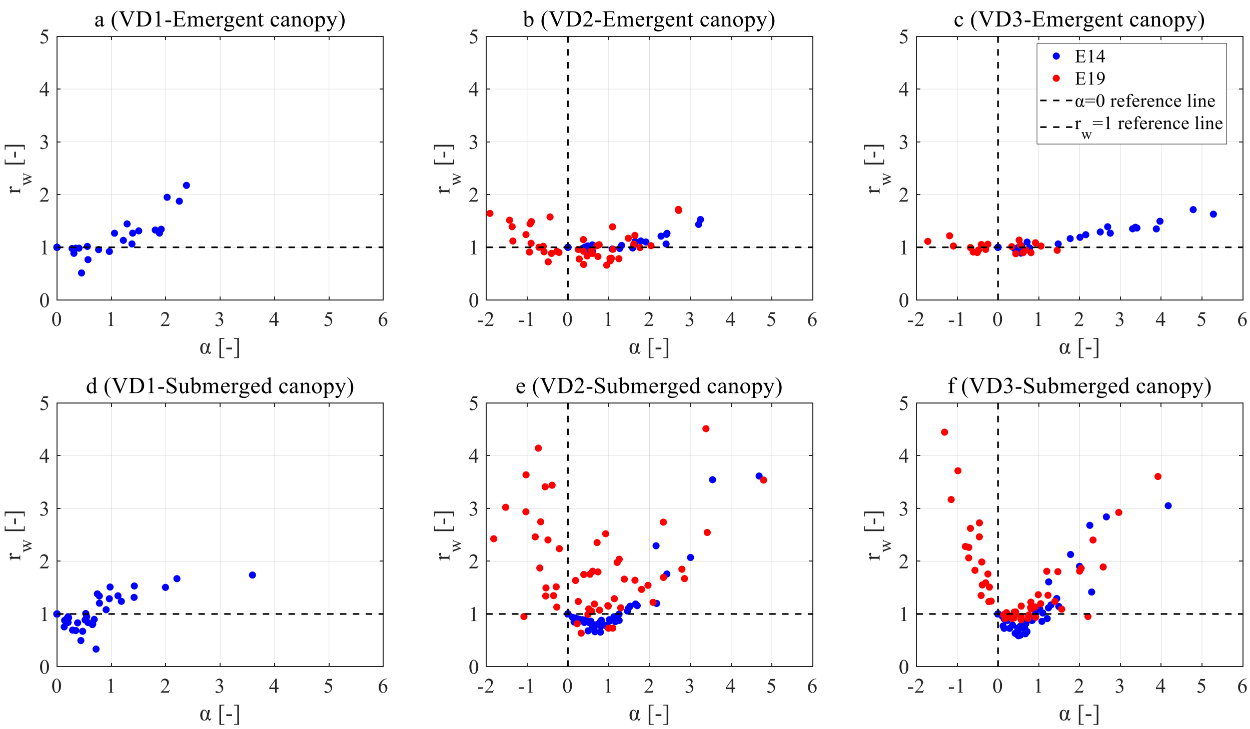

Figure 3. Relation between velocity ratios α and the relative decay r_w. (a), (b) and (c) show the variation of r_w with α in emergent canopies with stem densities of VD1, VD2 and VD3, respectively. (d), (e) and (f) show the variation of r_w with α in submerged canopies with stem densities of VD1, VD2 and VD3, respectively. The E14 data points are redrawn from Hu et al., (2014) with permission of Elsevier.

3.2 Velocity and force data

Velocity profiles reveal large difference in flow structures between different cases with various submergence and co-existing current conditions (Figure 4). A few similar patterns can be observed from both experiments: 1) the direction of U_{mean} is determined by the imposed current velocity; 2) in submerged canopies with co-existing currents, a distinctive velocity shear layer can be observed near the top of the vegetation canopy, whereas in emergent canopies velocity profiles are generally uniform; 3) the existence of vegetation reduces U_{mean} magnitude comparing to the control VD0 case. 4) when comparing wave-only and wave-current cases, the presence of wave leads to lower U_{mean} magnitude, regardless of the direction of the currents; 5) negative U_{mean} can be found in pure wave condition, which plays an important role in WDV variation as pointed out in the theoretical model in Hu et al., (2014).

https://doi.org/10.5194/essd-2021-180
Preprint. Discussion started: 21 June 2021

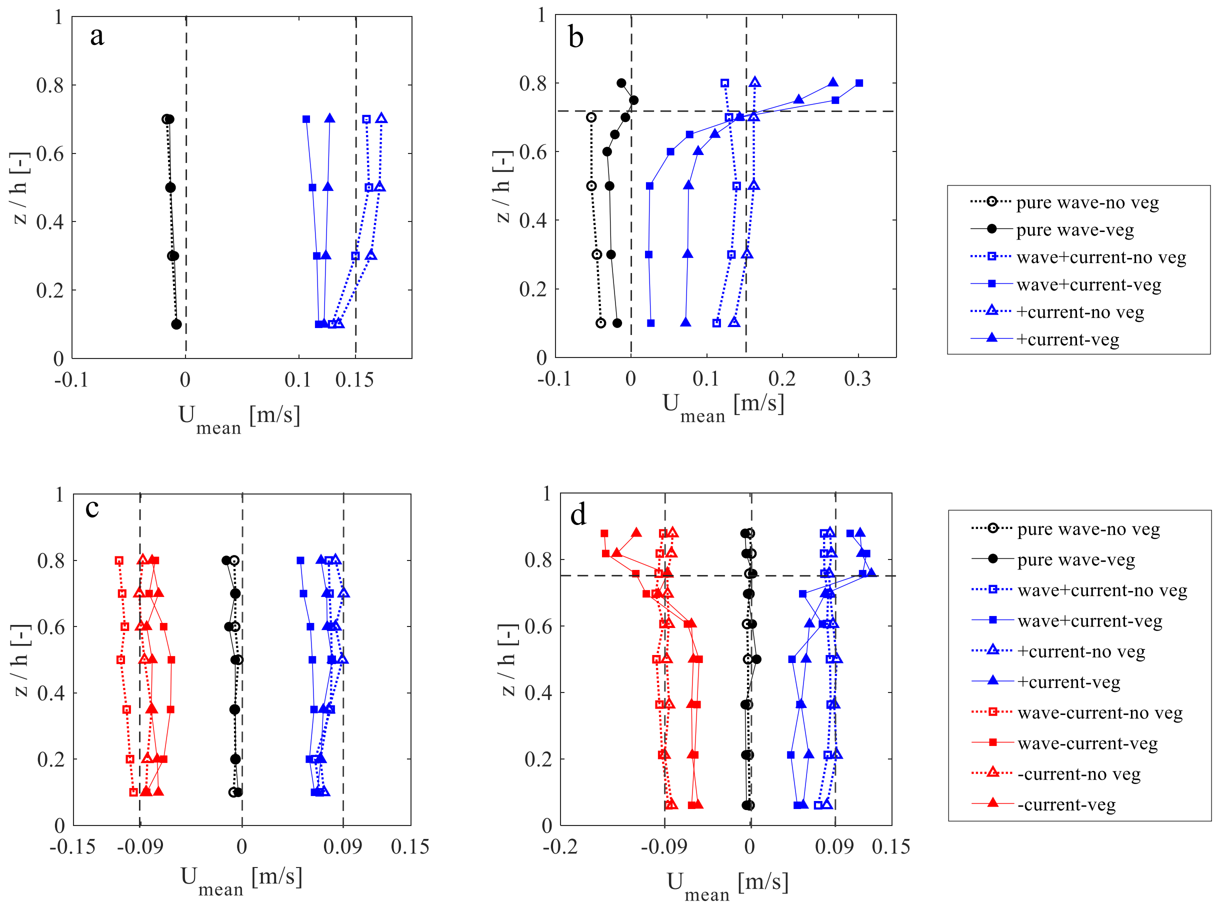

Figure 4. Vertical profile of time-mean velocity (U_{mean}). (a) emergent canopy with incident wave height of 6 cm and wave period of 1.2 s (i.e. wave0612) in E14; (b) submerged canopy with case wave1518 in E14; (c) emergent canopy with case wave0508 in E19; (d) submerged canopy with case wave0508 in E19. The E14 data points are redrawn from Hu et al., (2014) with permission of Elsevier.

Apart from the vertical velocity variation, we also include the raw data of the temporal variations of velocity (u) and the acting force (F) on vegetation mimics at multiple locations along vegetation canopies for all the tested cases (Figure 5). At each location, velocity and force measurements were taken at the same cross section. However, time lags still exist between the velocity and force data, which can be perceived via the phase difference between u peak and drag force peak (Figure 5d). These time lags may be induced by small misalignments between the ADV probes and the force sensor as well as the intrinsic delays of these instruments. To reduce the time lags and facilitate deriving C_D, an automatic algorithm is applied to synchronize u and F data, i.e. reducing the time lags between the peaks of u and F_D (Figure 5e). As a validation of the synchronization, the computed F_D (using derived C_D) and F_M signals is used to compose a reproduced F, which is subsequently compared with the

https://doi.org/10.5194/essd-2021-180
Preprint. Discussion started: 21 June 2021

measured total force. A comprehensive comparison shows that the calculated F is consistent with the measured total force (see Figure C1).

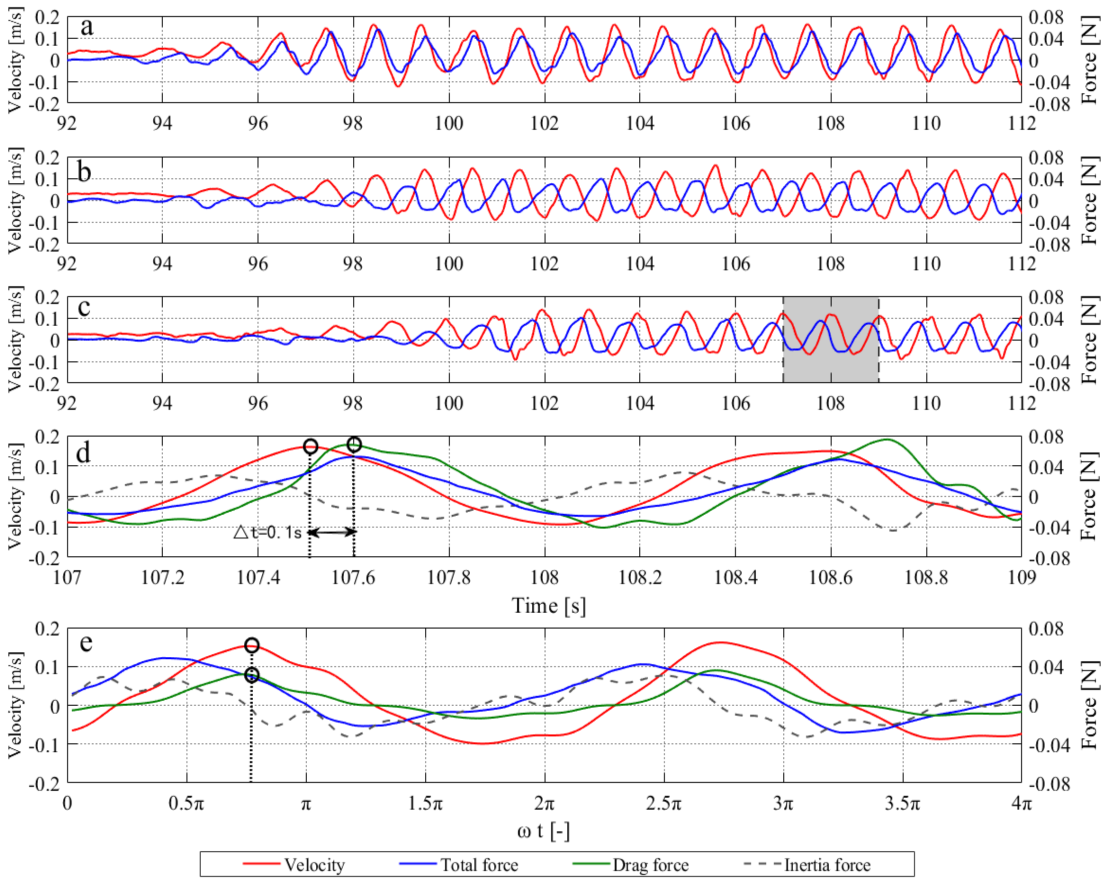

Figure 5. Synchronized velocity and force time series. (a-c) raw velocity and total force data measured at three locations in E19 in the order of wave propagation; (d) detailed data in the shaded area of (c), which shows the time shift (Δt) between u and F_D is about 0.1 s. (e) synchronized velocity and force data following the method of Yao et al., (2018). The shown test case is with 5 cm wave height, 1.0 s wave period and 0.03 m/s following current.

3.3 Drag coefficients

Our combined dataset shows an overall reduction trend of C_D with KC number across all the conditions of vegetation density, submergence ratio and co-existing currents (Figure 6). In E19, C_D reduces fast when KC increases from close to zero to 10. When the KC number approaches 20, C_D is reduced quickly to about 2. As the KC number increases above 20, C_D further reduces and finally reach a nearly constant value of 1.30. It is noted that the variation of C_D in opposing currents is the similar to that of following currents. There is no apparent difference between the two experiments, except that E14 contains a wider range of KC compared to E19 (Figure 6b). A C_D-KC relation for combined E14 and E19 data is listed below:

$$C_D = 0.95 + 11.39KC^{-1.09}, R^2 = 0.7222 \quad (8)$$

https://doi.org/10.5194/essd-2021-180
Preprint. Discussion started: 21 June 2021

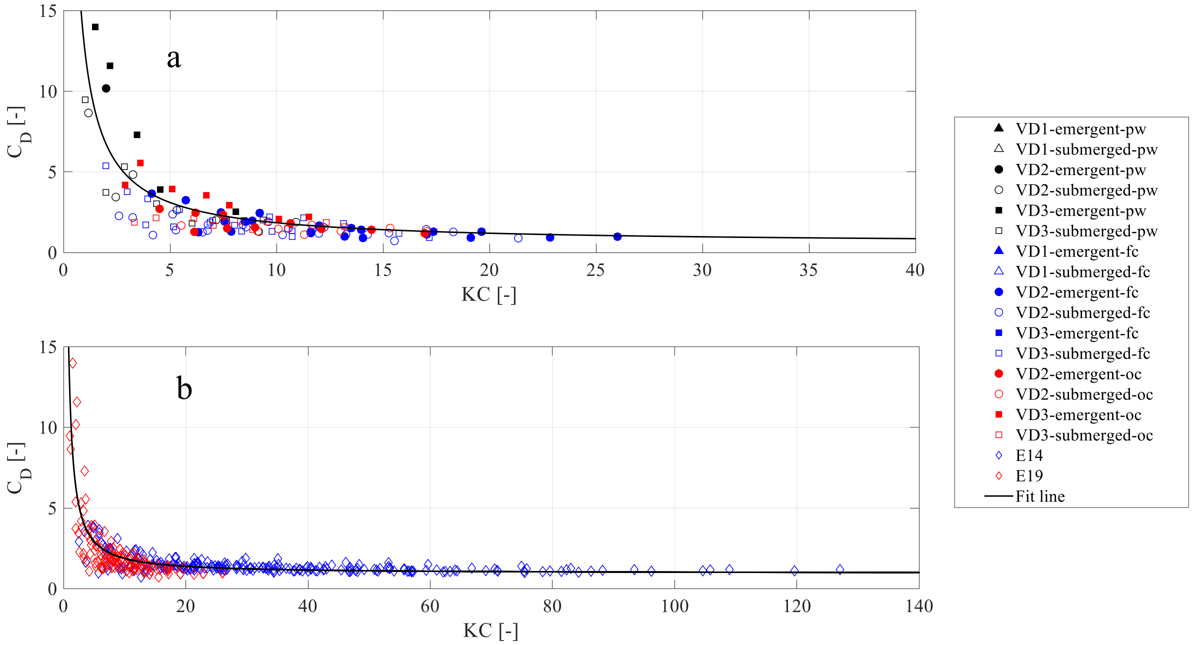

Figure 6. Relation between *KC* and C_D. (a) C_D in E19 with cases of pure wave ('pw'), wave with following current ('fc') and wave with opposing current ('oc'); (b) combined C_D in both E14 and E19. C_D were derived using the direct measurement approach (Appendix C).

4 Recommendations for Data Reuse

4.1 Towards a uniform drag coefficient relation

Our dataset includes a wide range of C_D in pure wave and wave-current flows. Base on such dataset, we derived a uniform C_D-*KC* empirical relation covering various combined wave-current conditions with both following and opposing currents. We reveal that C_D in opposing currents is also negatively correlated to *KC*, similar to other flow conditions. The C_D data with opposing currents are new supplementary to the existing studies. The resulting empirical relation can be valuable to the modelling of WDV, as the C_D relation derived in E14 has been successful applied in a number of theoretical and numerical studies (Henry et al., 2015; Hu et al., 2019; Suzuki et al., 2019). We expect this comprehensive empirical relation can assist future studies of WDV specially for those considering opposing currents. The current dataset also includes in-canopy velocity, acting force and temporal varying C_D. These data can be useful in assessing the force on vegetation stems and estimating e.g. survival of a mangrove canopy in storm events. lastly, as our experiments have tested numerous cases with varying canopy density, water depth and current-wave conditions, the generated dataset is thus suitable for machine learning quest, as such approach can be capable of deriving more sophisticated relations from multidimensional and nonlinear data (Tinoco et al., 2015; Goldstein et al., 2019).

4.2 Theoretical and model development of WDV in combined current-wave flows

Our experiments provide a unique dataset of wave height variation through vegetation with co-existing following and opposing currents. It show that co-existing currents have a substantial impact on WDV. They can reduce WDV by nearly 50% or increase WDV by 4 times depending on current velocity ratio (α). Thus, the effect of currents should account for in adequate WDV assessment. Our data reveal two general patterns of the wave dissipation trend with co-existing currents. First, WDV is suppressed or not sufficiently enhanced when the co-existing current velocity is small, but it is promoted when the current velocity is high, regardless of the imposed velocity direction. Second, in submerged canopies, opposing currents are more likely to promote WDV compared to following currents. Notably, cases with small following currents have the lowest WDV in both experiments. Therefore, to ensure safety, these cases should be regarded as the critical condition in designing nature-based coastal defense projects (Temmerman et al., 2013).

The presented dataset does not include tests of flexible vegetation (e.g. saltmarshes and seagrass) nor vegetation with root or leaves (He et al., 2019; Maza et al., 2019). The current dataset is expected to expand with additional WDV data in real mangrove wetlands from ongoing and future observation. While future experiments can certainly benefit from more realistic vegetation characteristics, the current dataset is still valuable in supporting the development of theoretical and numerical models (Losada et al., 2016; Suzuki et al., 2019), as the simplified setting of vegetation canopy facilitates in-depth investigation of complex wave-current-stem interactions. Such development may eventually aid the assessment and application of coastal vegetation wetland as a measure for coastal defense.

5 Data availability and future observations

All data presented in this paper are available from figshare (https://doi.org/10.6084/m9.figshare.13026530.v2; Hu et al., 2020). The repository includes data as well as instructions in readme files. Additionally, we expect that the current repository will expand with additional WDV data from ongoing as well as planned future observation in real mangrove wetlands, e.g. from ANCODE project (https://www.noc.ac.uk/projects/ancode).

Acknowledgments and Data

This work is supported by ANCODE (Applying nature-based coastal defense to the world's largest urban area—from science to practice) project, a three-way international funding through the Chinese National Natural Science Foundation (NSFC, Grant 51761135022), the Netherlands Organization for Scientific Research (NWO, lead funder, Grant ALWSD.2016.026), and the U.K. Research Councils (UKRI Grant EP/R024537/1), a project from National Natural Science Foundation of China (No. 51609269) and Guangdong Provincial Department of Science and Technology (2019ZT08G090). The data presented in this paper is freely accessible at https://doi.org/10.6084/m9.figshare.13026530.v2.

Author contribution

ZH, LS, HW and YL conducted the experiments and collected the raw data. ZH, MS and TS designed the experiments. ZH, LS and YL prepared the manuscript with contributions from all authors.

Competing interests

The authors declare that they have no conflicts of interest.

References

Arkema, K. K., Griffin, R., Maldonado, S., Silver, J., Suckale, J., and Guerry, A. D.: Linking social, ecological, and physical science to advance natural and nature-based protection for coastal communities, Ann. N. Y. Acad. Sci., 1399, 5–26, https://doi.org/10.1111/nyas.13322, 2017.

Borsje, B. W., Vries, S. de, Janssen, S. K. H., Luijendijk, A. P., and Vuik, V.: Building with nature as coastal protection strategy in the Netherlands, in: Living shorelines: The science and management of nature-based coastal protection, edited by: Bilkovic, D. M., Mitchell, M. M., La Peyre, M. K., and Toft, J. D., CRC Press, New York, 137–156, 2017.

Bouma, T. J., De Vries, M. B., Low, E., Peralta, G., Tánczos, I. C., Van De Koppel, J., and Herman, P. M. J.: Trade-offs related to ecosystem engineering: A case study on stiffness of emerging macrophytes, Ecology, 86, 2187–2199, 2005.

Cao, H., Feng, W., Hu, Z., Suzuki, T., and Stive, M. J. F.: Numerical modeling of vegetation-induced dissipation using an extended mild-slope equation, Ocean Eng., 110, 258–269, https://doi.org/10.1016/j.oceaneng.2015.09.057, 2015.

Chen, H., Ni, Y., Li, Y., Liu, F., Ou, S., Su, M., Peng, Y., Hu, Z., Uijttewaal, W., and Suzuki, T.: Deriving vegetation drag coefficients in combined wave-current flows by calibration and direct measurement methods, Adv. Water Resour., 122, 217–227, https://doi.org/10.1016/j.advwatres.2018.10.008, 2018.

Currin, C. A.: Chapter 30 - Living Shorelines for Coastal Resilience, in: Coastal Wetlands, edited by: Perillo, G. M. E., Wolanski, E., Cahoon, D. R., and Hopkinson, C. S., Elsevier, 1023–1053, https://doi.org/10.1016/B978-0-444-63893-9.00030-7, 2019.

Dalrymple, R., Kirby, J., and Hwang, P.: Wave Diffraction Due to Areas of Energy Dissipation, J. Waterw. Port Coast. Ocean Eng., 110, 67–79, https://doi.org/10.1061/(ASCE)0733-950X(1984)110:1(67), 1984.

Dean, R. and Dalrymple, R.: Water Wave Mechanics for Engineers and Scientists, World Scientific, Tokyo, 1991.

Garzon, J. L., Maza, M., Ferreira, C. M., Lara, J. L., and Losada, I. J.: Wave Attenuation by Spartina Saltmarshes in the Chesapeake Bay Under Storm Surge Conditions, J. Geophys. Res.-Oceans, 124, 5220–5243, https://doi.org/10.1029/2018JC014865, 2019.

Goldstein, E. B., Coco, G., and Plant, N. G.: A review of machine learning applications to coastal sediment transport and morphodynamics, Earth-Sci. Rev., 194, 97–108, https://doi.org/10.1016/j.earscirev.2019.04.022, 2019.

He, F., Chen, J., and Jiang, C.: Surface wave attenuation by vegetation with the stem, root and canopy, Coast. Eng., 152, 103509, https://doi.org/10.1016/j.coastaleng.2019.103509, 2019.

Henry, P.-Y., Myrhaug, D., and Aberle, J.: Drag forces on aquatic plants in nonlinear random waves plus current, Estuar. Coast. Shelf Sci., 165, 10–24, https://doi.org/10.1016/j.ecss.2015.08.021, 2015.

Hu, J., Hu, Z., and Liu, P. L.-F.: Surface water waves propagating over a submerged forest, Coast. Eng., 152, UNSP 103510, https://doi.org/10.1016/j.coastaleng.2019.103510, 2019.

Hu, Z., Suzuki, T., Zitman, T., Uijttewaal, W., and Stive, M.: Laboratory study on wave dissipation by vegetation in combined current-wave flow, Coast. Eng., 88, 131–142, https://doi.org/10.1016/j.coastaleng.2014.02.009, 2014.

Hu, Z.; Lian, S.; Wei, H.; Li, Y.; Uijttewaal, W.; Suzuki, T.: A dataset on wave propagation through vegetation with coexisting currents. figshare. Dataset. https://doi.org/10.6084/m9.figshare.13026530.v2, 2020

Jadhav, R. S., Chen, Q., and Smith, J. M.: Spectral distribution of wave energy dissipation by salt marsh vegetation, Coast. Eng., 77, 99–107, https://doi.org/10.1016/j.coastaleng.2013.02.013, 2013.

Lara, J. L., Maza, M., Ondiviela, B., Trinogga, J., Losada, I. J., Bouma, T. J., and Gordejuela, N.: Large-scale 3-D experiments of wave and current interaction with real vegetation. Part 1: Guidelines for physical modeling, Coast. Eng., 107, 70–83, https://doi.org/10.1016/j.coastaleng.2015.09.012, 2016.

Lei, J. and Nepf, H.: Blade dynamics in combined waves and current, J. Fluids Struct., 87, 137–149, https://doi.org/10.1016/j.jfluidstructs.2019.03.020, 2019.

Leonardi, N., Camacina, I., Donatelli, C., Ganju, N. K., Plater, A. J., Schuerch, M., and Temmerman, S.: Dynamic interactions between coastal storms and salt marshes: A review, Geomorphology, 301, 92–107, https://doi.org/10.1016/j.geomorph.2017.11.001, 2018.

Li, C. W. and Yan, K.: Numerical investigation of Wave - Current - Vegetation interaction, J. Hydraul. Eng., 133, 794–803, https://doi.org/10.1061/(ASCE)0733-9429(2007)133:7(794), 2007.

van Loon-Steensma, J. M., Slim, P. A., Decuyper, M., and Hu, Z.: Salt-marsh erosion and restoration in relation to flood protection on the Wadden Sea barrier island Terschelling, J. Coast. Conserv., 1–16, https://doi.org/10.1007/s11852-014-0326-z, 2014.

van Loon-Steensma, J. M., Hu, Z., and Slim, P. A.: Modelled Impact of Vegetation Heterogeneity and Salt-Marsh Zonation on Wave Damping, J. Coast. Res., 32, 241–252, https://doi.org/10.2112/JCOASTRES-D-15-00095.1, 2016.

Losada, I. J., Maza, M., and Lara, J. L.: A new formulation for vegetation-induced damping under combined waves and currents, Coast. Eng., 107, 1–13, https://doi.org/10.1016/j.coastaleng.2015.09.011, 2016.

Maza, M., Lara, J. L., Losada, I. J., Ondiviela, B., Trinogga, J., and Bouma, T. J.: Large-scale 3-D experiments of wave and current interaction with real vegetation. Part 2: Experimental analysis, Coast. Eng., 106, 73–86, https://doi.org/10.1016/j.coastaleng.2015.09.010, 2015.

Maza, M., Lara, J. L., and Losada, I. J.: Experimental analysis of wave attenuation and drag forces in a realistic fringe Rhizophora mangrove forest, Adv. Water Resour., 131, UNSP 103376, https://doi.org/10.1016/j.advwatres.2019.07.006, 2019.

Méndez, F. J. and Losada, I. J.: An empirical model to estimate the propagation of random breaking and nonbreaking waves over vegetation fields, Coast. Eng., 51, 103–118, 2004.

Möller, I., Kudella, M., Rupprecht, F., Spencer, T., Paul, M., van Wesenbeeck, B. K., Wolters, G., Jensen, K., Bouma, T. J., Miranda-Lange, M., and Schimmels, S.: Wave attenuation over coastal salt marshes under storm surge conditions, Nat. Geosci., 7, 727–731, https://doi.org/10.1038/ngeo2251, 2014.

https://doi.org/10.5194/essd-2021-180
Preprint. Discussion started: 21 June 2021

Morison, J. R., Johnson, J. W., and Schaaf, S. A.: The Force Exerted by Surface Waves on Piles, J. Pet. Technol., 2, 149–154, https://doi.org/10.2118/950149-G, 1950.

Nepf, H. M.: Flow Over and Through Biota, in: Treatise on Estuarine and Coastal Science, edited by: Wolanski, E. and McLusky, D., Academic Press, Waltham, 267–288, 2011.

Paul, M., Bouma, T. J., and Amos, C. L.: Wave attenuation by submerged vegetation: -combining the effect of organism traits and tidal current, Mar. Ecol. Prog. Ser., 444, 31–41, https://doi.org/10.3354/meps09489, 2012.

Pujol, D., Serra, T., Colomer, J., and Casamitjana, X.: Flow structure in canopy models dominated by progressive waves, J. Hydrol., 486, 281–292, https://doi.org/10.1016/j.jhydrol.2013.01.024, 2013.

Stewart, H. L.: Hydrodynamic consequences of maintaining an upright posture by different magnitudes of stiffness and buoyancy in the tropical alga Turbinaria ornata, J. Mar. Syst., 49, 157–167, https://doi.org/10.1016/j.jmarsys.2003.05.007, 2004.

Stratigaki, V., Manca, E., Prinos, P., Losada, I. J., Lara, J. L., Sclavo, M., Amos, C. L., Cáceres, I., and Sánchez-Arcilla, A.: Large-scale experiments on wave propagation over Posidonia oceanica, J. Hydraul. Res., 49, 31–43, https://doi.org/10.1080/00221686.2011.583388, 2011.

Suzuki, T., Hu, Z., Kumada, K., Phan, L. K., and Zijlema, M.: Non-hydrostatic modeling of drag, inertia and porous effects in wave propagation over dense vegetation fields, Coast. Eng., 149, 49–64, https://doi.org/10.1016/j.coastaleng.2019.03.011, 2019.

Temmerman, S., Meire, P., Bouma, T. J., Herman, P. M. J., Ysebaert, T., and De Vriend, H. J.: Ecosystem-based coastal defence in the face of global change, Nature, 504, 79–83, https://doi.org/10.1038/nature12859, 2013.

Tinoco, R. O., Goldstein, E. B., and Coco, G.: A data-driven approach to develop physically sound predictors: Application to depth-averaged velocities on flows through submerged arrays of rigid cylinders, Water Resour. Res., 51, 1247–1263, https://doi.org/10.1002/2014WR016380, 2015.

Tinoco, R. O., San Juan, J. E., and Mullarney, J. C.: Simplification bias: lessons from laboratory and field experiments on flow through aquatic vegetation, Earth Surf. Process. Landf., 45, 121–143, https://doi.org/10.1002/esp.4743, 2020.

Vuik, V., Jonkman, S. N., Borsje, B. W., and Suzuki, T.: Nature-based flood protection: The efficiency of vegetated foreshores for reducing wave loads on coastal dikes, Coast. Eng., 116, 42–56, https://doi.org/10.1016/j.coastaleng.2016.06.001, 2016.

Yao, P., Chen, H., Huang, B., Tan, C., Hu, Z., Ren, L., and Yang, Q.: Applying a New Force-Velocity Synchronizing Algorithm to Derive Drag Coefficients of Rigid Vegetation in Oscillatory Flows, Water, 10, 906, https://doi.org/10.3390/w10070906, 2018.

https://doi.org/10.5194/essd-2021-180
Preprint. Discussion started: 21 June 2021

Appendix A. Photos of the experiment instruments and setup

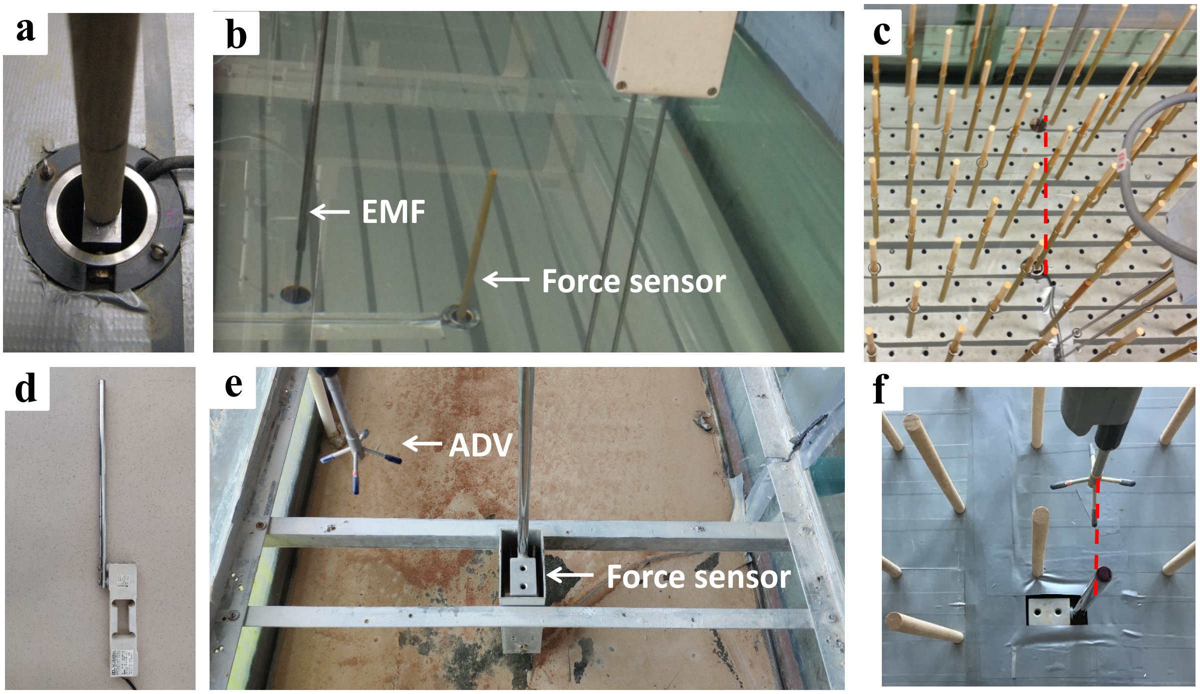

Figure A1. Photos of the applied instruments and canopy arrangement in E14 (a-c) and E19 (d-f). In E14, (a) force sensors and (b) EMFs (electromagnetic flow manufacture meters) for velocity measurement were developed by Deltares (former Delft Hydraulics, the Netherlands). In E19, (d) force sensors were model M104 developed by UTILCELL and (e) ADVs (acoustic doppler velocimeter) for velocity measurement were from Nortek. (c) and (f) show that the force and velocity measurements were taken at the same transect of the flume to obtain synchronized data.

Appendix B. Test conditions in the two experiments

Table B1 shows the tested cases in both E14 and E19. A large number of tests were included in both experiments: 314 in E14 and 366 in E19. In all the tests, the wave height spatial variation, in-canopy force and velocity were measured. Each test was conducted at least twice to ensure reproducibility. For a few selected cases, the velocity profiles were measured by moving the EMF or ADV measuring probe vertically in the water column.

In E14, the selected cases were wave0612 and wave1518. For emergent canopy cases (h=0.25 m), the velocity was measured at 4 locations: z/h=0.1, 0.3, 0.5 and 0.7. In submerged canopy cases (h=0.50m), u was measured at 8 locations: z/h=0.1, 0.3, 0.5, 0.6, 0.65, 0.75, 0.8 and 0.9. The measuring location was refined near the top of the canopy (h_v/h = 0.72). In E19, the selected cases were wave0508. For emergent canopy cases (h=0.20 m), the velocity was measured at 7 locations: z/h=0.2, 0.3, 0.4, 0.5, 0.65, 0.75 and 0.9. In submerged canopy cases (h=0.33m), u was measured at 9 locations: z/h=0.12, 0.18, 0.24, 0.30, 0.39, 0.5, 0.63, 0.79 and 0.94.

https://doi.org/10.5194/essd-2021-180
Preprint. Discussion started: 21 June 2021

Table B1. Test conditions in E14 and E19 with different combinations of hydrodynamic conditions and mimic canopy configurations

Source	Water depth (h)/plant height (h_v)	Stem density (N) [#/m^2]	Wave height (H) [m]	Wave period (T) [s]	Wave case	Co-existing current velocity direction and magnitude (U_c) [m/s]
E14	0.25/0.36	62/139/556	0.04	1.0	Wave0410[a]	0/+0.05/+0.15/+0.20
		62/139/556	0.04	1.2	Wave0412	0/+0.05/+0.15/+0.20
		62/139/556	0.06	1.0	Wave0610	0/+0.05/+0.15/+0.20
		62/139/556	0.06	1.2	Wave0612	0/+0.05/+0.15/+0.20
		62/139/556	0.08	1.2	Wave0812	0/+0.05/+0.15/+0.20
		62/139/556	0.08	1.5	Wave0815	0/+0.05/+0.15/+0.20
		62/139/556	0.10	1.5	Wave1015	0/+0.05/+0.15/+0.20
	0.50/0.36	62/139/556	0.04	1.0	Wave0410	0/+0.05/+0.15/+0.20/+0.30[b]
		62/139/556	0.06	1.2	Wave0612	0/+0.05/+0.15/+0.20/+0.30
		62/139/556	0.08	1.4	Wave0814	0/+0.05/+0.15/+0.20/+0.30
		62/139/556	0.10	1.6	Wave1016	0/+0.05/+0.15/+0.20/+0.30
		62/139/556	0.12	1.6	Wave1216	0/+0.05/+0.15/+0.20/+0.30
		62/139/556	0.12	1.8	Wave1218	0/+0.05/+0.15/+0.20/+0.30
		62/139/556	0.15	1.6	Wave1516	0/+0.05/+0.15/+0.20/+0.30
		62/139/556	0.15	1.8	Wave1518	0/+0.05/+0.15/+0.20/+0.30
		62/139/556	0.15	2.0	Wave1520	0/+0.05/+0.15/+0.20/+0.30
		62/139/556	0.18	2.2	Wave1822	0/+0.05/+0.15/+0.20/+0.30
		62/139/556	0.20	2.5	Wave2025	0/+0.05/+0.15/+0.20/+0.30
E19	0.20/0.25	139/556	0.03	0.6	Wave0306	0/±0.03/±0.06/±0.09/±0.12/±0.15
		139/556	0.03	0.8	Wave0308	0/±0.03/±0.06/±0.09/±0.12/±0.15
		139/556	0.05	0.6	Wave0506	0/±0.03/±0.06/±0.09/±0.12/±0.15
		139/556	0.05	0.8	Wave0508	0/±0.03/±0.06/±0.09/±0.12/±0.15
		139/556	0.05	1.0	Wave0510	0/±0.03/±0.06/±0.09/±0.12/±0.15
	0.33/0.25	139/556	0.03	0.6	Wave0306	0/±0.03/±0.06/±0.09/+0.12/+0.15
		139/556	0.03	0.8	Wave0308	0/±0.03/±0.06/±0.09/+0.12/+0.15
		139/556	0.05	0.6	Wave0506	0/±0.03/±0.06/±0.09/+0.12/+0.15
		139/556	0.05	0.8	Wave0508	0/±0.03/±0.06/±0.09/+0.12/+0.15
		139/556	0.05	1.0	Wave0510	0/±0.03/±0.06/±0.09/+0.12/+0.15
		139/556	0.07	0.8	Wave0708	0/±0.03/±0.06/±0.09/+0.12/+0.15
		139/556	0.07	1.0	Wave0710	0/±0.03/±0.06/±0.09/+0.12/+0.15

[a] wave0410 means the incident regular wave height is 4 cm and the wave period is 1.0 s.

[b] '+' means current flow in the same direction of waves, '-' means current flow in the opposite direction of waves; in E14, the low vegetation density tests (62 stems/m^2) does not have '+0.30 m/s' cases.

https://doi.org/10.5194/essd-2021-180
Preprint. Discussion started: 21 June 2021

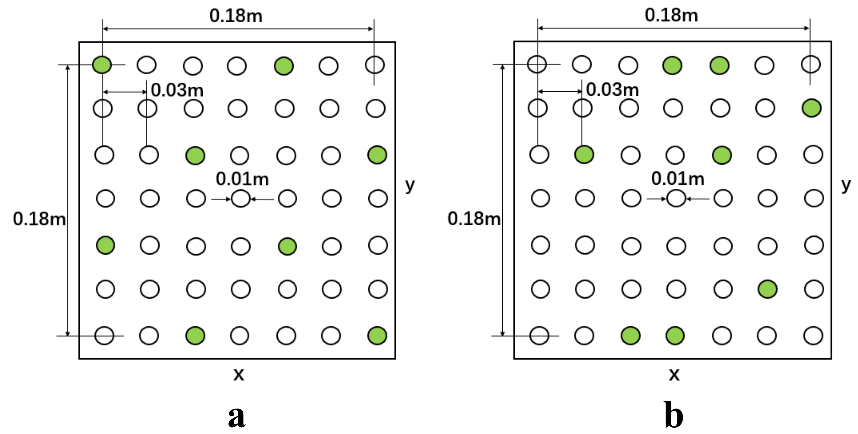

Figure B1. top view of vegetation mimics distribution in E19 (a) regular canopy, 139 stems/m^2; (b) random canopy, 139 stems/m^2

Appendix C. Direct measurement method of C_D

The direct measurement method of C_D in combined current-wave flows was first introduced in Hu et al., (2014) and it was further improved in Yao et al., (2018). Such method is proposed for both pure wave and combined wave-current flows. The force acting on an individual mimic stem is composed of drag force and inertia force, as expressed by Morison equation (Eq. 1, Morison et al., 1950)

The only unknown parameter in Morison equation is drag coefficient C_D. To derive period-averaged C_D, the direct measurement method applies the technique of quantifying the work done by the acting force (Hu et al., 2014). The work done by the acting force on mimic stem over a full wave period is composed of the work done by the drag force and the inertia force, expressed as:

$$W = W_D + W_M = \frac{1}{T}\int_0^T F_D u dt + \frac{1}{T}\int_0^T F_M u dt \tag{C1}$$

where W_D and W_M are the work performed by F_D and F_M over a wave period, respectively. Since W_M equals to zero in both pure wave and current-wave conditions, F_M doesn't contribute to the WDV (Dalrymple et al., 1984). Hence W equals to W_D. Therefore, the period-averaged C_D can be derived based on the following equation:

$$C_D = \frac{2\int_0^T F_D u dt}{\int_0^T \rho h_v b_v u^2 |u| dt} = \frac{W_D}{\int_0^T \rho h_v b_v u^2 |u| dt} = \frac{\mathrm{W}}{\int_0^T \rho h_v b_v u^2 |u| dt} = \frac{2\int_0^T F u dt}{\int_0^T \rho h_v b_v u^2 |u| dt} \tag{C2}$$

Before applying direct measurement to derive C_D, the force data and velocity data should be aligned (Figure 5d). Detailed procedure of alignment can be found in Yao et al., (2018). As drag force (F_D) is a function of velocity (u) Eq. (1), F_D and u should be in the same phase. By using measured total force (F), measured velocity (u) and the inertia coefficient (C_M) into Eq. (1), we can obtain the drag force (F_D) and then adjust the phase shift (Δt) between the velocity and drag force peaks. The obtained new velocity and force data time series will be used as inputs in the next run. This loop is excecated over 30 times.

https://doi.org/10.5194/essd-2021-180
Preprint. Discussion started: 21 June 2021

Finally, the minimum phase shift (Δt) and the aligned velocity and force timeseries will be chosen as outputs for deriving C_D. As a validation of the directly derived C_D, we reproduced the maximum force ($F_{\text{cal-max}}$) in both positive and negative directions using the derived C_D, and compared it with the measured maximum force ($F_{mea\text{-}max}$, see Figure C1).

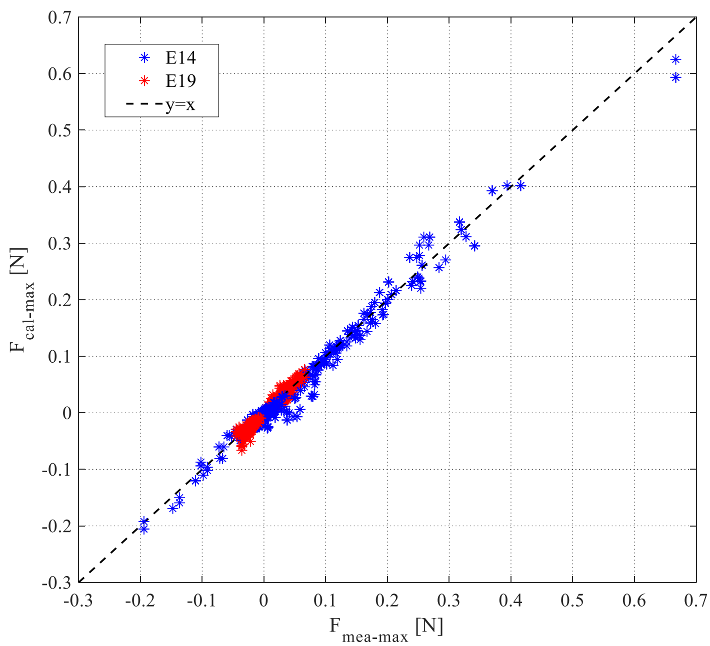

Figure C1. A comparison between measured maximum force ($F_{mea\text{-}max}$) and calculated maximum force ($F_{\text{cal-max}}$) in both positive and negative directions. $F_{\text{cal-max}}$ is reproduced using directly derived C_D.